

Charge and spin order in one-dimensional electron systems with long-range Coulomb interactions

B. Valenzuela

Instituto de Ciencia de Materiales, CSIC, Cantoblanco, E-28049 Madrid, Spain

S. Fratini

*Laboratoire d'Etudes des Propriétés Electroniques des Solides, CNRS,
25 avenue des Martyrs, BP 166, F-38042 Grenoble Cedex 9, France*

D. Baeriswyl

Département de Physique, Université de Fribourg, Pérolles, CH-1700 Fribourg, Switzerland

(Dated: December 30, 2021)

We study a system of electrons interacting through long-range Coulomb forces on a one-dimensional lattice, by means of a variational ansatz which is the strong-coupling counterpart of the Gutzwiller wave function. Our aim is to describe the quantum analogue of Hubbard's classical "generalized Wigner crystal". We first analyse charge ordering in a system of spinless fermions, with particular attention to the effects of lattice commensurability. We argue that for a general (rational) number of electrons per site n there are three regimes, depending on the relative strength V of the long-range Coulomb interaction (as compared to the hopping amplitude t). For very large V the quantum ground state differs little from Hubbard's classical solution, for intermediate to large values of V we recover essentially the Wigner crystal of the continuum model, and for small V the charge modulation amounts to a small-amplitude charge-density wave. We then include the spin degrees of freedom and show that in the Wigner crystal regimes (i.e. for large V) they are coupled by an antiferromagnetic kinetic exchange J , which turns out to be smaller than the energy scale governing the charge degrees of freedom. Our results shed new light on the insulating phases of organic quasi-1D compounds where the long-range part of the interaction is unscreened, and magnetic and charge orderings coexist at low temperatures.

I. INTRODUCTION

Compounds that are poor electrical conductors or insulators often exhibit charge patterns which differ from the homogeneous charge distribution encountered in ordinary metals. The charge ordering often occurs at a relatively high temperature and is accompanied by a magnetic ordering at a lower temperature. These phenomena are quite generic, as they are observed in a variety of systems. Important examples are the three-dimensional nickelates, the layered cuprates at specific commensurate fillings, layered molecular crystals such as BEDT-TTF radical salts and quasi-one-dimensional systems such as the organic TMTTF and DCNQI compounds. From a theoretical point of view, the full long-ranged Coulomb potential should in principle be included when dealing with *any* interacting insulating phase, due to the ineffectiveness of screening. Accordingly, it is not surprising to find wide classes of apparently different compounds showing similar behaviours in their insulating phases. In this respect, the possibility that the two phenomena of charge and spin ordering share a common origin is very appealing. Yet, it is not obvious that the two separate energy scales can be described within the same physical mechanism.

This raises the question of determining a set of unambiguous signatures of the long-range Coulomb interactions, to be compared with the experiments. One such signature is of course charge ordering itself, as was first

recognised by Wigner in the framework of the three-dimensional electron gas.¹ In the low-density limit, the kinetic energy of the electrons becomes negligible and the charges arrange themselves in the form of a *Wigner lattice* which minimizes the electrostatic energy. However, it is sometimes difficult to determine whether the observed charge modulation is induced by long-range forces or by an instability of the Fermi surface. Moreover, even if the main driving mechanism is given by the Coulomb forces, the presence of other effects (elastic, magnetic) in real compounds can strongly modify the predicted ordering pattern.

When applying the idea of Wigner crystallization to electrons in narrow-band solids, we are faced with the additional constraint that the charges must sit on the sites of a discrete lattice (the *host* lattice of atoms, to be distinguished from the Wigner crystal of electrons). This has been pointed out by Hubbard,² who considered the extreme limit of zero bandwidth, a sensible starting point if the dominant energy scale is set by the interactions.

In the present work, we propose a variational treatment which allows to go beyond the classical limit by including the effects of quantum fluctuations. Our results indicate that for small but finite hopping parameters, the charge and spin degrees of freedom are energetically decoupled: charge crystallization, governed by the (large) Coulomb energy, naturally gives rise to antiferromagnetic spin correlations, characterised by a much smaller energy scale. The coexistence of charge and spin

ordering at low energies can thus be considered as distinctive of dominant long-range Coulomb interactions, and should therefore be ubiquitous in the insulating phases of strongly interacting systems.

It can be argued that for special fillings, short-range models with one or few interaction parameters (e.g. the Hubbard model for half-filled bands, or the extended Hubbard model for quarter-filled bands) can give a correct description of the system. Although they give the right answer for the ground state charge configuration for special fillings, the strong-coupling analysis presented here shows that these models can no longer be applied as soon as the filling deviates from such special values, since in this case they do not yield the proper classical ground state (a system with purely local interactions is metallic away from half-filling). Therefore, a complete understanding of the behaviour of the insulating phases as a function of the density can only be achieved by taking into account the long range part of the Coulomb potential.

We study a system of fermions in one dimension, interacting via a local repulsion U and a long-ranged Coulomb potential $V_m = V/|m|$, m being the distance between electrons. The corresponding tight-binding Hamiltonian on an L -site ring is

$$\hat{H} = -t\hat{T} + U\hat{D} + V\hat{W} \quad (1)$$

where we have defined the following dimensionless operators, describing respectively electron hopping, on-site and long-range repulsion,

$$\hat{T} = \sum_{n\sigma, s=\pm 1} c_{n\sigma}^+ c_{n+s\sigma} \quad , \quad (2)$$

$$\hat{D} = \sum_i n_{i\uparrow} n_{i\downarrow} \quad , \quad (3)$$

$$\hat{W} = \frac{1}{2} \sum_{i \neq j \sigma \sigma'} \frac{n_{i,\sigma} n_{j,\sigma'}}{|i-j|} \quad , \quad (4)$$

$c_{i,\sigma}^+$ ($c_{i,\sigma}$) creates (destroys) an electron of spin σ at site i , $n_{i,\sigma} = c_{i,\sigma}^+ c_{i,\sigma}$ is the occupation number of this state and t is the hopping amplitude between nearest-neighbor sites.

The paper is organized as follows. In the next section we introduce our variational wave function, starting from Hubbard's solution for the classical limit. In Section III, we study the phenomenon of charge ordering at different commensurate fillings by neglecting the magnetic degrees of freedom. These are analysed for a quarter-filled band in Section IV, where contact is also made with experimental results for organic quasi-one-dimensional compounds.

II. VARIATIONAL WAVE FUNCTION FOR GENERALIZED WIGNER LATTICES

The limit studied by Hubbard² is obtained by setting the bandwidth to zero and $U \rightarrow \infty$. In this case

the problem is classical (but still non-trivial), and corresponds to minimising the interaction energy by distributing the N electrons as homogeneously as possible over the L available lattice sites. The difficulty arises from the competition between the different interaction parameters V_m . If the potential is convex, as in the Coulomb case, a solution can be found for any commensurate filling $n = N/L = r/s$ (r and s integers) in the form of the generalized Wigner lattice (GWL), a periodic sequence of unit cells of size s , each containing r electrons distributed according to a minimum spread of interelectron distances. The charge density on site l is either 1 or 0 according to the following formula:³

$$n_l = [lr/s] - [(l-1)r/s] \quad (5)$$

where $[\dots]$ gives the integer part of the argument.

For finite t quantum fluctuations will tend to delocalize the electrons away from the classical configuration. Nevertheless, the classical solution is still a good approximation for small t where most of the charge is located on the sites predicted by eq. (5). This argument can be made more precise for simple fillings $n = 1/s$. Moving a particle away from the classical configuration costs an energy

$$\Delta = 2V \sum_{m=1}^{\infty} \frac{1}{ms[(ms)^2 - 1]} \quad . \quad (6)$$

A density $\delta n \sim (t/\Delta)^2$ will thus be allowed to leak to the nearest unoccupied sites. The charge gap is $\Delta = 0.39V$ at quarter filling ($n = 1/2$) and is rapidly reduced at lower fillings, $\Delta \simeq 2.4n^3V$, since the repulsion that prevents the occupation of "wrong" sites weakens as the inter-electron distance increases. The range of validity of the classical approximation can be estimated by requiring δn to be smaller than a threshold value P . This leads to the phenomenological criterion that quantum band motion has negligible effects as long as V exceeds the value

$$V_{GWL} \approx \frac{t}{2.4\sqrt{P}n^3} \quad . \quad (7)$$

Note that $V_{GWL} \sim n^{-3}$, so that it is harder to stabilize a classical GWL at low densities, where V_{GWL} can be very large. Taking for instance $P = 0.2$, eq. (7) gives $V_{GWL}/t \approx 8$ at $n = 1/2$ and $V_{GWL}/t \approx 500$ at $n = 1/8$.²⁸

In order to study the ground state of the full Hamiltonian (1) we now use the variational ansatz

$$|\Psi_B(\eta)\rangle = e^{-\eta\hat{T}}|\Psi_\infty\rangle \quad , \quad (8)$$

introduced previously as the strong coupling counterpart of the Gutzwiller wave function in the context of the Mott-Hubbard transition⁴. Here η is a dimensionless variational parameter, \hat{T} is the kinetic energy operator of eq. (2) and $|\Psi_\infty\rangle$ is the ground state for $t = 0$, i.e. Hubbard's classical solution. In the same way as the Gutzwiller wave function reduces double occupancy and

thus states with high potential energy, the factor $e^{-\eta\hat{T}}$ suppresses configurations with high kinetic energy.

It can be demonstrated that the wave function (8) is charge ordered and insulating for any finite η — its charge stiffness, or equivalently, its Drude weight, vanishes.⁵ A transition to a metallic state occurs for $\eta \rightarrow \infty$, where only the configuration with the lowest kinetic energy, i.e. the filled Fermi sea, survives. $|\Psi_B\rangle$ is expected to provide a fairly accurate description of charge fluctuations in the strong coupling limit, but it can no longer be trusted for weak couplings, although it tends to the correct limit as the interaction vanishes.²⁹

Our wave function is easy to handle for $U \rightarrow \infty$ where spin fluctuations are suppressed and the problem becomes equivalent to that of spinless fermions. In this case, our variational procedure can be used straightforwardly to study not only simple fillings such as $n = 1/2$ but also much more complex GWL ground states such as $n = 11/47$, and it can readily be generalized to higher dimensions. For finite values of U , where spin fluctuations have to be taken into account, the problem becomes more complicated. However, in the strong coupling limit $U, V \gg t$ the energy scales for charge and spin degrees of freedom are very different, and the problem of magnetic ordering can be addressed in terms of a low-energy spin Hamiltonian, in fact the simple antiferromagnetic Heisenberg model for the case $n = 1/2$. This will be discussed in section IV.

III. SPINLESS FERMIONS

We shall first assume that the on-site repulsion is the dominant energy scale, and take the limit $U \rightarrow \infty$. This eliminates both double occupancy and mixing of different spin configurations. We can therefore suppress the spin index in the Hamiltonian (1)-(4), and ignore the local term (3). Transforming to Fourier space leads to the following simplified model for *spinless* electrons:

$$\hat{H} = -t\hat{T} + V\hat{W} = \sum_k \epsilon_k c_k^\dagger c_k + \frac{1}{2L} \sum_q V(q) \rho_q \rho_{-q} \quad (9)$$

where the band dispersion relation is $\epsilon_k = -2t \cos k$, $\rho_q = \sum_k c_{k+q}^\dagger c_k$ is the density fluctuation operator, and $V(q) = -V \log[2(1 - \cos q)]$ (the lattice parameter has been set equal to 1). The q sums run over the entire Brillouin zone except $q = 0$, which ensures charge neutrality. To avoid multiple counting of the interaction energy, we have taken the limit $L \rightarrow \infty$ with the prescription that the range of the interaction potential does not exceed half the length of the ring.³⁰ The Coulomb potential has a logarithmic singularity at long wavelengths, characteristic of the one-dimensional case, and an intrinsic cut-off at short wavelengths given by the lattice parameter.

The wave function (8) can be worked out exactly for any filling $n = r/s$. We shall present in full detail the formalism for $n = 1/2$. Results will be given for different fillings as well.

A. Filling $n = 1/2$

The classical solution in this case corresponds to alternating occupied and empty sites. This can be written in k -space as:

$$|\Psi_\infty\rangle = \prod_{k \in RBZ} \frac{1}{\sqrt{2}} (c_k^\dagger + c_{k+\pi}^\dagger) |0\rangle \quad (10)$$

where the product runs over the reduced Brillouin zone $|k| < \pi/2$, and $|0\rangle$ is the vacuum for electrons. The phase correlator $e^{-\eta\hat{T}}$ is now diagonal and we can write straightforwardly the (normalized) variational wave function (8) as

$$|\Psi_B(\eta)\rangle = \prod_{k \in RBZ} \frac{1}{N_k} (e^{-\eta\epsilon_k} c_k^\dagger + e^{\eta\epsilon_k} c_{k+\pi}^\dagger) |0\rangle \quad (11)$$

where the normalization factor is given by $N_k^2 = 2 \cosh(2\eta\epsilon_k)$ (we have set $t = 1$ so that energies are now expressed in units of the hopping parameter). The best variational ground state is obtained by minimising the energy functional

$$E_B(\eta) = \langle \Psi_B(\eta) | \hat{H} | \Psi_B(\eta) \rangle \quad (12)$$

with respect to the variational parameter. The kinetic energy per unit length is readily evaluated

$$\langle \hat{T} \rangle / L = \int_{RBZ} \frac{dk}{2\pi} \epsilon_k \tanh(2\eta\epsilon_k). \quad (13)$$

The potential energy can be expressed in terms of the structure factor $S(q) = \langle \rho_q \rho_{-q} \rangle / L$,

$$\langle V\hat{W} \rangle / L = \frac{1}{4\pi} \int dq S(q) V(q). \quad (14)$$

The structure factor has a regular part

$$S(q) = \frac{1}{4} - \frac{1}{4\pi} \int_{RBZ} dk \frac{1 + \sinh(2\eta\epsilon_k) \sinh(2\eta\epsilon_{k-q})}{\cosh(2\eta\epsilon_k) \cosh(2\eta\epsilon_{k-q})} \quad (15)$$

and a Bragg peak at $q = \pi$ corresponding to the periodic ordering of the charges:

$$S(\pi) = L \left[\int_{RBZ} \frac{dk}{2\pi} \frac{1}{\cosh(2\eta\epsilon_k)} \right]^2. \quad (16)$$

Writing the average density distribution as $n(l) = n + \tilde{n} \cos(\pi l)$, we see that the intensity of the Bragg peaks in the structure factor is proportional to the square of the order parameter, $S(\pi)/L = \tilde{n}^2$. It is finite for any finite η , so that the wave function $|\Psi_B\rangle$ always represents a charge-ordered state.

In the limit $\eta \rightarrow 0$ one recovers the classical GWL. The kinetic energy vanishes and the structure factor becomes $S(q) = (1/4)\delta_{q,\pi}$, so that equation (12) gives $E_{cl} = V(\pi)/8 = -(V/4) \log 2$. The opposite limit $\eta \rightarrow \infty$

yields the Hartree–Fock energy of the liquid phase, which is equivalent to treating the interaction to lowest order in perturbation theory. Equation (15) then gives $S(q) = |q|/2\pi$ and one readily evaluates $E_0(V) = -2/\pi - cV$, with $c = 7\zeta(3)/8\pi^2 = 0.10657$ (ζ is the Riemann function). For finite η , one can define the condensation energy as the energy gained through charge ordering, $E_{cond} = E_B - E_0$. This quantity is shown in figure 1 as a function of V . The variational result (full line) is very close to the Hartree-Fock result in the broken-symmetry phase (dashed line). The latter is known to be a good approximation in the strong coupling regime, and is surprisingly accurate in the presence of lattice commensurability, which strongly reduces charge fluctuations.⁶ Although no

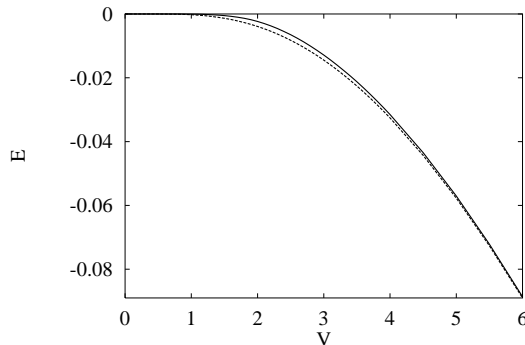


FIG. 1: Total condensation energy (per unit volume) for spinless fermions at $n = 1/2$ as a function of the interaction strength V (energies are in units of t).

phase transition occurs within our variational approach, there is a crossover between a weak-coupling regime, where the density modulation is small as compared to the average density, and a strong-coupling (or classical) regime, where the order parameter approaches the limiting value of Hubbard’s GWL pattern. Correspondingly, the condensation energy is exponentially small at low V , behaving like $E_{cond} \simeq -0.02V \exp(-2\pi/V)$, while at large V it can be expanded in powers of t/V as $E_{cond} \approx 0.64t - 0.067V - 2.59t^2/V + \dots$

A direct indication on how the charge modulation builds up is given by the evolution of the structure factor, shown in figure 2. At $V = 1$ (top line) $S(q)$ is very close to the structure factor of non-interacting electrons. Upon increasing V , the regular part is progressively reduced, and some weight is transferred to the Bragg peak (see the inset, full line). Despite a marked onset around $V \approx t$, $S(\pi)$ is still far from its classical limit (indicated by an arrow) at values as high as $V = 10t$. The variational result for a model with only nearest-neighbour interactions (dashed line) shows that for equal values of V in the charge-ordered regime, the long-range nature of the Coulomb potential *reduces* the amplitude of charge ordering, because the energy cost for creating a local charge fluctuation is partly compensated by the interaction parameters V_m at distances $m > 1$.³¹ This is in agreement

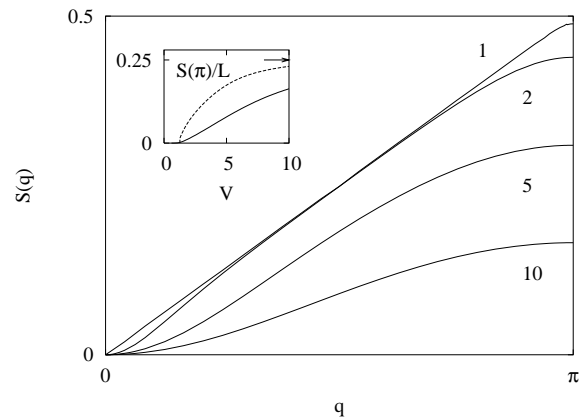


FIG. 2: Structure factor in the spinless case for different values of the interaction strength at $n = 1/2$: from top to bottom, $V = 1, 2, 5, 10t$. The inset shows the intensity of the Bragg peak at π , proportional to the square of the order parameter, versus V . The dashed line is the same quantity evaluated in a model with only nearest neighbour interactions. The arrow marks the classical limiting value.

with refs.⁷, where it is shown that the metallic character of the system is enhanced when going from short (i.e. nearest-neighbor) to long-range interactions.

B. General rational fillings

For generic commensurate fillings of the form $n = r/s$, the s harmonics needed to reproduce the GWL pattern produce s Bragg peaks in the Brillouin zone at multiples of $2\pi/s$ (for even s , the points $\pm\pi$ of the Brillouin zone are equivalent). It is straightforward to extend the analysis presented above for $r = 1$, $s = 2$ to larger values of s .

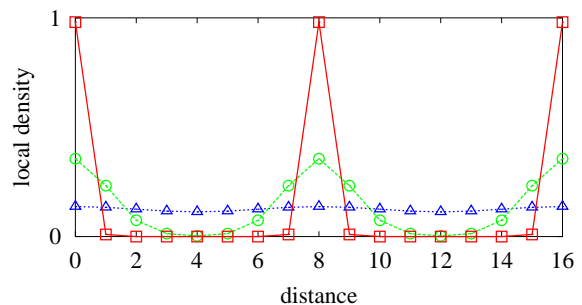


FIG. 3: Average occupation of site l for different values of the interaction strength at $n = 1/8$: $V = 0.5t$ (triangles), $V = 20t$ (circles), $V = 500t$ (squares). Lines are guides to the eye.

Figure 3 shows the variational results for the average site occupation at a filling $n = 1/8$, for different values of the interaction strength. Unlike the case $n = 1/2$, which exhibits a single crossover from weak to strong coupling, three different regimes can now be identified. (I)

For $V/t = 0.5$ (triangles) the modulation of the density is weak. (II) For larger values of the coupling strength ($V/t = 20$, circles), the charge modulation is strong, and the total wave function is essentially made up of localised one-electron wave functions with virtually no overlap, like in an ordinary Wigner crystal. The GWL (III), where only the sites predicted by Hubbard's solution are occupied, is achieved only at extremely large V ($V/t = 2000$, squares).

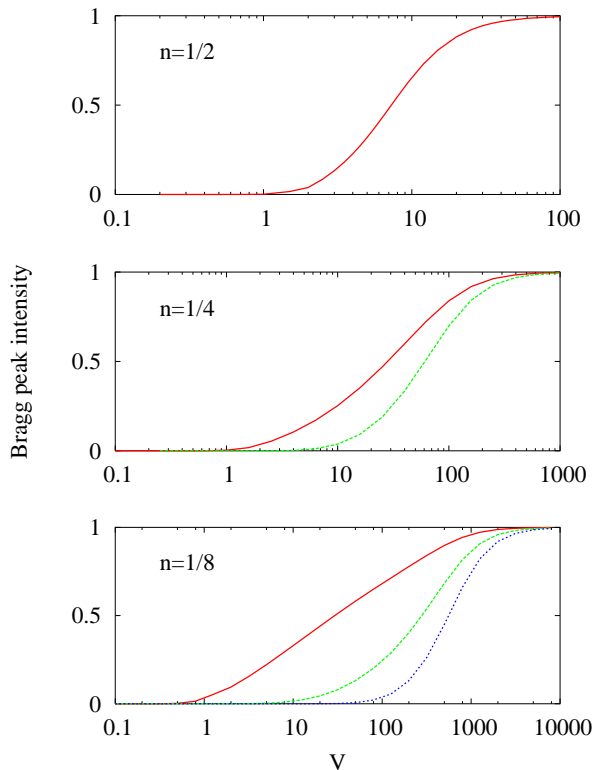


FIG. 4: Normalised intensities of the Bragg peaks at multiples of $q_{WC} = 2\pi n$, versus the interaction strength. From top to bottom: $n = 1/2, 1/4, 1/8$. The full, dashed and dotted lines correspond respectively to first, second and third harmonics. Note the different scale in the three graphs.

Figure 4 shows the normalised intensities of the peaks in the structure factor at multiples of $q_{WC} = 2\pi n$, namely $S(\nu q_{WC})/n^2 L$, as a function of the coupling strength, for $n = 1/2$ (top), $1/4$ (center) and $1/8$ (bottom). We see that at fillings $n < 1/2$, higher harmonics progressively appear in the structure factor when increasing the coupling, in addition to the main peak at q_{WC} . The system goes progressively from the weak coupling limit (I), where the modulation can be described in terms of a single, exponentially small, Bragg peak, to the GWL (III), where all the harmonics in the structure factor saturate to their classical value. Note that the intermediate region (II) becomes broader as n decreases.

C. From the Wigner lattice to the pinned charge-density wave

By construction, our variational wave function exhibits long-range order for any finite positive value of η (and thus for any positive value of V in the case of the long-range Coulomb interaction). The evolution of the charge modulation proceeds smoothly from a *GWL* at very large V over an ordinary Wigner crystal at large but not too large V to a small-amplitude charge-density wave from intermediate to small values of V . However, it is obviously not clear whether a trial wave function which is linked to the exact ground state for $t/V = 0$ can still be trusted in a region where $V/t < 1$, since in this case it would be more appropriate to start from the filled Fermi sea.

To examine this point, we consider the soluble model of 1D spinless fermions with nearest-neighbor interaction (parameter V). For an average occupation $n = 1/2$ this model is equivalent to the *XXZ* Heisenberg chain in zero magnetic field with exchange constants $J_x/J_z = J_y/J_z = 2t/V$. For $V > 2t$ (uniaxial regime for the spin chain) there is true long-range order, but not for $V < 2t$ (planar regime). The absence of long-range order for small values of V can also be understood within the Fermi gas model, where the (crystal) lattice generates an Umklapp term; the latter has to exceed a certain critical strength in order to sustain long-range charge order⁸. Our wave function predicts long-range order for $V > V_c \approx 1.3t$ and a weak first-order transition to a metallic phase for $V = V_c$ (see the inset of figure 2). Thus the predictions of our variational ansatz agree qualitatively with the exact phase diagram.

The question of the existence of true long-range order for 1D lattice fermions interacting through the $1/r$ Coulomb potential, i.e., for the Hamiltonian (9), is more subtle and still not completely understood. In the absence of a lattice potential, Schulz⁹ has shown, using bosonization for small V and an analysis of quantum fluctuations about the classical Wigner crystal at large V , that the long-distance behavior of the density-density correlation function is universally given by

$$\langle \rho(x)\rho(0) \rangle \sim A \cos(Qx) e^{-c\sqrt{\log(x)}}, \quad (17)$$

where $Q = 2k_F$ for the spinless model ($4k_F$ for model (1) with $U = \infty$) and the constant c is independent of V . Thus Wigner crystallization in the sense of quasi-long-range order exists independently of the interaction strength in one dimension. This is in sharp contrast to three and two space dimensions, where Wigner crystallization is known to take place at *finite* values of the interaction strength¹⁰, namely at $r_s \simeq 100$ and $r_s \simeq 37$, respectively (r_s is defined as the radius of a sphere containing one electron in average, expressed in units of the Bohr radius, and controls the potential/kinetic energy ratio).

One expects that any additional commensurate lattice potential will transform the quasi-long-range order into

a true long-range order. This has been confirmed on the basis of exact diagonalization⁷ for large V and $n = 1/3$. For small V , estimates of the effects of Umklapp scattering (using bosonization⁷) are also in line with the existence of a finite order parameter, although its value and the corresponding lattice pinning energy are expected to be extremely small.

In contrast to bosonization, which cannot provide the amplitude of the density–density correlation function [the strongly interaction–dependent constant A in Eq. (17)], our variational approach allows us to estimate the order parameter as a function of both the interaction strength V and the average site occupation n . In 1D the dimensionless parameter of the continuum theory is $r_s = (a/2n)/a_B$. Within the tight-binding model (9), the dispersion ϵ_k close to the band edges can be approximated by a parabola with an effective mass $m^* = \hbar^2/(2ta^2)$. Using the unscreened Coulomb potential for V and inserting the band mass m^* into the definition of the Bohr radius, i.e., $a_B = 2ta/V$, one obtains

$$r_s = \frac{V}{4nt} . \quad (18)$$

Starting from the Wigner crystal phase (II), where the electron wave functions are well separated (cf. fig. 3), and varying V , we expect to encounter two crossovers, the first to a weakly pinned charge–density wave upon decreasing V , the second to a GWL upon increasing V . The first crossover towards a weakly modulated ground state takes place when the spread σ of the single–particle wavefunctions equals a given fraction δ of the average inter–particle distance $d = 1/n$, namely

$$\frac{\sigma}{d} \approx \delta . \quad (19)$$

In our lattice problem, the spread of the single–particle wave functions can be defined as

$$\sigma^2 = \sum_{l=-d/2}^{d/2} l^2 n_l \quad (20)$$

(the origin has been chosen to coincide with an occupied site of the GWL). The Lindemann criterion (19) is expected to locate a broad crossover region rather than a true phase transition in the present 1D case. Therefore the choice of δ is somehow arbitrary, and we shall take $\delta = 0.25$.

We have calculated the crossover V_{Lind} predicted by the Lindemann criterion (19) for various fillings $n = 1/32, 1/16, 1/8, 1/4$ and $1/2$. Remarkably, the values obtained at low fillings ($n < 1/4$) scale linearly with n , as expected from continuum theory in view of eq. (18), corresponding to a crossover around $r_s \approx 2.5$. The situation changes at fillings $n = 1/4$ and $n = 1/2$, where the increasing influence of lattice effects favors localization of the particles, thus reducing the value of r_s at the crossover ($r_s \approx 2$ at $n = 1/2$, see also ref.⁶). As to the

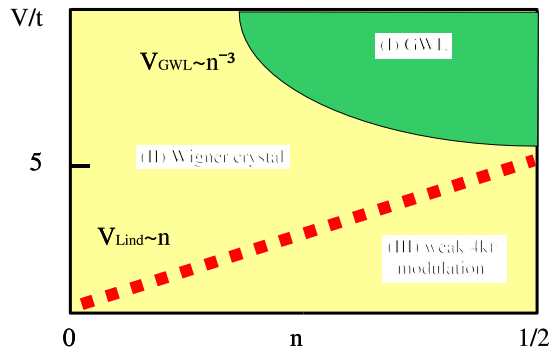


FIG. 5: Phase diagram for the spinless model (9). A charge-ordered state persists for all commensurate fillings with three characteristic regimes, from top to bottom: (I) generalized Wigner lattice, (II) Wigner crystal and (III) small-amplitude charge–density wave.

crossover towards the GWL, we may use the criterion (7), i.e. $V_{GWL} \sim n^{-3}$.

The resulting phase diagram is shown in figure 5, where the two boundaries represent the two crossover regions for rational fillings $n = 1/s$, s integer. Starting from Hubbard’s classical GWL at $V \rightarrow \infty$ (top), the inclusion of quantum fluctuations at a given density n gives rise to two successive crossovers. First, around V_{GWL} the particles begin to spill over to the neighboring lattice sites, and the ground state becomes similar to the Wigner crystal of the continuum model. Reducing further the interaction strength progressively suppresses the higher harmonics of the density modulation, so that below the second crossover around V_{Lind} only a small-amplitude “ $4k_F$ ” charge–density wave remains.

These crossover lines have opposite density dependences. $V_{GWL} \sim n^{-3}$ decreases with increasing density, since reducing the inter–particle distance makes it easier to confine particles on a single lattice site. $V_{Lind} \sim n$ increases with density, since the potential/kinetic energy ratio scales as $V/(nt)$ [eq. (18)]. At $n = 1/2$, where lattice effects are most important, $V_{GWL} \approx V_{Lind}$ and the two crossovers become indistinguishable: the Wigner crystal phase is wiped out, and the system passes directly from the classical GWL to the weakly modulated phase. Note that in the spinless case presented here, there is full particle–hole symmetry relative to $n = 1/2$, which allows to deduce the phase diagram for $1/2 < n < 1$.

D. Fluctuations of polarization

An insulator, such as our electronic system with a commensurate charge–ordered ground state, responds to an applied electric field E by a macroscopic polarization

$P = \langle \hat{X}/L \rangle$, where

$$\hat{X} = \sum_l l n_l \quad (21)$$

is the dipole operator and we have set the electron charge equal to unity. The dielectric susceptibility is defined as $\chi = P/E$ in the limit $E \rightarrow 0$. The upper bound¹¹

$$\chi \leq \frac{2}{L\Delta} \langle \hat{X}^2 \rangle \quad (22)$$

links χ to the mean-square fluctuation of polarization $\langle \hat{X}^2 \rangle$ (we have taken $\langle \hat{X} \rangle = 0$ by symmetry) and to the charge gap Δ (defined here as the minimum excitation energy for which the dipole matrix element does not vanish). In a Wigner solid the electrons are located close to their classical equilibrium positions and each one contributes an amount σ^2 [cf. eq. (20)] to the mean-square deviation of polarization, giving

$$\frac{\langle \hat{X}^2 \rangle}{L} \approx n \sigma^2 \quad (23)$$

According to the discussion of the previous section, the properties of the system in region II (the region of the conventional Wigner crystal) should agree with the predictions of continuum theory. Therefore, when plotted as a function of r_s , the quantity $(\sigma/d)^2 = n \langle \hat{X}^2 \rangle / L$ evaluated at different fillings should fall on a *universal curve*. The results at $n = 1/16$ (asterisks), $n = 1/8$ (circles), $n = 1/4$ (squares) and $n = 1/2$ (triangles) are plotted in fig. 6, showing indeed a scaling behavior up to the value $V_{GWL}(n)$, indicated by arrows. On the left side of the figure, the crossover between the Wigner crystal phase (II) and the weakly modulated regime (I) is signaled by a marked upturn of the curve around $r_s \approx 2$, which is roughly filling independent (except for $n = 1/2$), and agrees with the phenomenological Lindemann criterion (19).

The scaling behavior breaks down when we enter the GWL region (III), i.e. at V_{GWL} . The onset depends on the filling, so that the scaling region is progressively reduced as n increases, and it completely disappears at $n = 1/2$, where lattice effects are most important. Note that at this particular filling the fluctuations of polarization are systematically reduced with respect to the universal curve (the reduction is approximately 30% around $r_s \approx 2$), showing that lattice commensurability favors charge localization. Above V_{GWL} (on the right side of the figure), where the charges become localized on individual sites, there is a rapid drop in the fluctuations of polarization, and it can be shown following the perturbative arguments of section II that $(\sigma/d)^2 \simeq 1/(46 r_s^2 n^6)$.

IV. MAGNETIC CORRELATIONS

The assumption of infinite U implies for the present one-dimensional case that the different spin configurations do not mix and that the magnetic exchange constant is zero. It follows that from a thermodynamic point

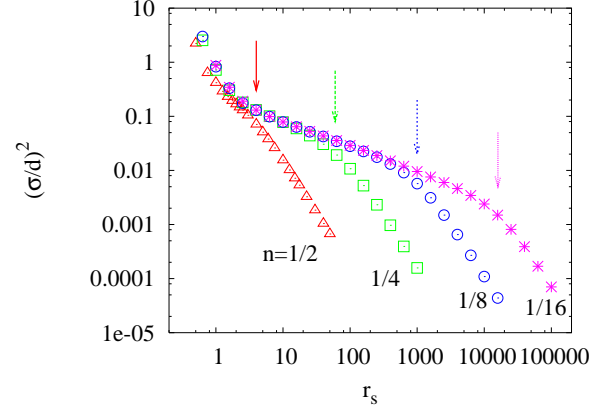


FIG. 6: The fluctuations of polarization as a function of $r_s = V/4nt$, for different fillings: $n = 1/16$ (asterisks), $n = 1/8$ (circles), $n = 1/4$ (squares) and $n = 1/2$ (triangles). Scaling breaks down when entering the GWL phase (marked by arrows), which is dominated by lattice effects.

of view the spins behave as free magnetic moments giving rise to a Curie-type magnetic susceptibility. In some of the organic materials such a behavior is indeed observed at temperatures where charge ordering sets in, but at lower temperatures antiferromagnetic correlations lead to a substantial reduction of the magnetic susceptibility and finally to a magnetically ordered ground state. In this section we show that our variational approach can be readily generalized to finite values of U . We limit ourselves to large Coulomb interactions, where the magnetic energy scale turns out to be much smaller than the energies associated with the charge ordering, and treat explicitly the quarter-filled case ($n = 1/2$), which is relevant for some quasi-one-dimensional compounds such as the TMTTF salts¹² or the DCNQI materials¹³ (for a collection of recent results see ref.¹⁴).

We consider the Hamiltonian (1) for large coupling constants, $U \gg t, V \gg t$. Since the variational ansatz (8) does not penalize configurations with doubly occupied sites, we use a refined wave function^{15,16}

$$|\Psi_{BG}\rangle = e^{-\lambda \hat{D}} e^{-\eta \hat{T}} |\Psi_\infty\rangle, \quad (24)$$

where $|\Psi_\infty\rangle$ is now a linear superposition of states that can be visualized in real space as

$$\left\{ \left| \begin{array}{cccccccc} \sigma_1 & 0 & \sigma_2 & 0 & \sigma_3 & 0 & \cdots & \sigma_N & 0 \end{array} \right\rangle \right\}. \quad (25)$$

(σ_i is the spin of a localized electron and zeroes stand for empty sites). Since the classical ground state is highly (2^N) degenerate, we do not introduce *a priori* any special magnetic order (e.g. antiferromagnetic or ferromagnetic) but we allow for all possible spin configurations. In the variational wave function (24) the term $e^{-\eta \hat{T}}$ again controls the delocalization of charge away from the generalized Wigner lattice (25) and $e^{-\lambda \hat{D}}$ reduces the weight of configurations with doubly occupied sites. As there is no

preferred spin configuration in the classical GWL, magnetic correlations will be generated exclusively by quantum fluctuations.

The energy of the ground state is obtained by minimizing the expression

$$E_{BG}(\lambda, \eta) = \frac{\langle \Psi_{BG} | \hat{H} | \Psi_{BG} \rangle}{\langle \Psi_{BG} | \Psi_{BG} \rangle} = \frac{\langle \Psi_{\infty} | e^{-\eta \hat{T}} e^{-\lambda \hat{D}} (-t \hat{T} + U \hat{D} + V \hat{W}) e^{-\lambda \hat{D}} e^{-\eta \hat{T}} | \Psi_{\infty} \rangle}{\langle \Psi_{\infty} | e^{-\eta \hat{T}} e^{-2\lambda \hat{D}} e^{-\eta \hat{T}} | \Psi_{\infty} \rangle} \quad (26)$$

with respect to the two variational parameters λ and η . Unlike what happens in the spinless case, a closed analytical expression for $E_{BG}(\lambda, \eta)$ has not been found. Instead, we use the expansion $e^{-\eta \hat{T}} \simeq 1 - \eta \hat{T} + \frac{1}{2} \eta^2 \hat{T}^2 + \dots$, which is valid for small η (i.e. small t).³² Each factor \hat{T} produces hopping to neighboring sites. Therefore, in order to allow for spin exchange, we have to expand at least to fourth order in η . The corresponding hopping processes are illustrated in figure 7. They lead to an

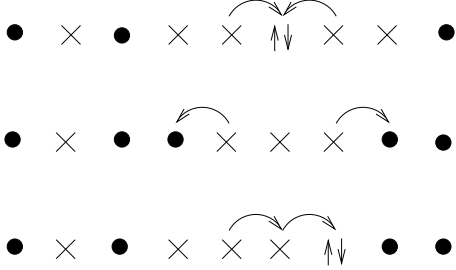


FIG. 7: Intermediate state contributing to the interaction energy at fourth order. Dots/crosses stand for filled/empty sites respectively. Notice that the first and third processes can give rise to spin exchange.

exchange of neighboring spins as shown explicitly in Appendix A, where the expectation values of the hopping term \hat{T} , of the number of doubly occupied sites \hat{D} and of the long-range part of the interaction \hat{W} are calculated to fourth order in η . Collecting the results of eqs. (A7), (A9) and (A14), we obtain the total energy

$$E_{BG}(\lambda, \eta) = L \left[-\frac{V}{4} \log 2 + 2\eta t + (2 \log 2 - 1) \eta^2 V \right] + J \sum_{i \text{ even}} \langle \Psi_{\infty} | \vec{S}_i \cdot \vec{S}_{i+2} - \frac{1}{4} n_i n_{i+2} | \Psi_{\infty} \rangle, \quad (27)$$

where the exchange constant J is given by

$$J = -4\eta^3 t (1 + 3e^{-\lambda}) - 3\eta^4 U e^{-2\lambda} - 4V \eta^4 \left[2 \log 2 - 1 + e^{-2\lambda} \left(2 \log 2 - \frac{15}{8} \right) \right]. \quad (28)$$

We see that the variational parameters η (which controls the delocalization of charge) and λ (which reduces double occupancy) can be determined independently of the spin configurations contributing to the magnetic

ground state, which depends only on the sign of the exchange constant. For antiferromagnetic exchange the ground state energy is given by¹⁷

$$\sum_{i \text{ even}} \langle \Psi_{\infty} | \vec{S}_i \cdot \vec{S}_{i+2} - \frac{1}{4} n_i n_{i+2} | \Psi_{\infty} \rangle = -\frac{L}{2} \log 2. \quad (29)$$

If the parameter η is small enough (which is certainly the case in the Wigner crystal phase), it is essentially determined by the minimum of the first term in eq. (27), i.e.

$$\eta \approx -\frac{t}{(2 \log 2 - 1)V}. \quad (30)$$

On the other hand, λ is chosen such as to maximize the exchange constant J , namely

$$e^{-\lambda} = -\frac{3t}{2\eta \left[\frac{3}{4}U + (2 \log 2 - \frac{15}{8})V \right]}. \quad (31)$$

Inserting these two values into eq. (28) we obtain

$$J \approx \frac{9t^4}{(2 \log 2 - 1)^2 V^2 \left[\frac{3}{4}U + (2 \log 2 - \frac{15}{8})V \right]}. \quad (32)$$

The resulting ground state energy per site

$$\frac{1}{L} E_{BG} = -\frac{V}{4} \log 2 - \frac{t^2}{(2 \log 2 - 1)V} - \frac{J}{2} \log 2 \quad (33)$$

consists of three terms, the energy of the classical Wigner crystal, the energy gain due to charge delocalization and the magnetic exchange energy.

We see here that the finiteness of U leads to an antiferromagnetic coupling between the spins, which is a direct consequence of the quantum fluctuations in the charge-ordered state. Recently it has been shown that the spin correlations in the Heisenberg chain decay like $(-1)^{(i-j)} (\log |i-j|)^{1/2} / |i-j|$.¹⁸ In the framework of our variational approach, the long-range order in the charge sector is therefore accompanied by an algebraic magnetic order.³³

The variational analysis presented above for $n = 1/2$ indicates that in the region where the approach is valid, $U \gg t, V \gg t$, there is a *separation of energy scales* between the charge and the spin degrees of freedom. Recently, charge ordering has been observed in the organic chain compounds (TMTTF)₂ PF₆ and (TMTTF)₂ AsF₆ at $T_{CO} = 70K$ and $100K$, respectively. No structural transition has been observed so far at T_{CO} and the magnetic ordering occurs at much lower temperatures (around $10K$). It is tempting to associate the charge ordering, which has been reported on the basis of both *NMR*¹⁹ and dielectric measurements,²⁰ with the stabilization of a Wigner lattice, although for a detailed comparison with experiments structural effects may have to be taken into account. Previously, experiments on (DI-DCNQI)₂Ag have already been interpreted in terms of a Wigner crystal.¹³

It has become popular to describe organic conductors in terms of the extended Hubbard model, where only on-site and nearest-neighbor Coulomb interactions with coupling constants U and V_1 , respectively, are taken into account.^{21,22,23} Informations about the parameter values can be obtained by exploiting the well-known sum rule relating the optical absorption to the total kinetic energy. For (TMTTF)₂PF₆ exact diagonalization studies for the kinetic energy reproduce the observed reduction of oscillator strength of 0.73²⁴ (as compared to that of non-interacting electrons) using the parameters $U = 8t$ and $V_1 = 3t$ or else $U = 6.7t$ and $V = 3.3t$ (see Fig. 4a in ref.²²). Our variational approach applied to the same model would give roughly the same values together with an exchange constant $J_1 = 6t^2/(UV_1^2) \approx 0.08t$. For long-range Coulomb interactions, which suppress the kinetic energy much less, the situation is quite different. In fact, for $n = 1/2$ and $U = 2V$, a reduction factor of 0.73 would require a Coulomb interaction strength of $V = 9t$. Nevertheless, the exchange constant, given by eq. (28) would again be of the order of 0.08t.

In addition to the simple case presented here, the study of more complex fillings can be envisaged. For instance, the GWL configuration 110110... at filling $n \simeq 2/3$, which is relevant to TTF-TCNQ, intrinsically leads to a dimerization of the exchange constants, and could result in qualitatively new physics. Our approach may also shed new light onto the $4k_F$ modulations observed in TTF-TCNQ²⁵ and in several 1:2 compounds. Most of the structural data exhibit a single harmonic modulation, so that they could be attributed to region (III) of the “phase diagram” of fig. 5.

V. CONCLUSION

We have studied a one-dimensional system of electrons interacting through the long-range Coulomb interaction on a discrete lattice. Starting from the charge-ordered classical limit, we have introduced a variational wave function which allows to treat the effects of quantum fluctuations. This wave function is always insulating and charge ordered at any commensurate filling, and is particularly well suited in the limit of strong interactions.

Although no phase transition arises within our treatment, the phase diagram can be clearly divided into three distinct regions separated by crossovers: (I) the classical generalized Wigner lattice in the limit where the band motion is negligible, (II) a Wigner crystal regime at intermediate couplings and (III) a weakly modulated regime at low interaction strengths. Lattice effects appear to be particularly important at simple commensurate fillings, where the charge fluctuations are reduced as compared to those of a continuous system. This general trend agrees with recent results obtained in two space dimensions,⁶ where it was shown that the critical parameter for Wigner crystallization is dramatically reduced from the value $r_s \approx 35$ in continuous models to $r_s \approx 2$ in

a quarter-filled band.

Concerning the spin degrees of freedom, exchange processes induced by quantum fluctuations were shown to give rise to antiferromagnetic correlations. These develop out of the charge ordered configuration, with a much lower characteristic energy scale than typical Coulomb interaction energies. For the quarter-filled band the spin sector has been mapped onto the antiferromagnetic Heisenberg chain, which exhibits algebraically decaying spin correlations.

The existence of a charge-ordered ground state, as well as the aforementioned decoupling of magnetic/charge energy scales, are not unique to long-range interactions. However, besides quantitative differences between the genuinely long-ranged and the *ad hoc* short-ranged models, taking into account the unscreened long-range Coulomb potential appears to be crucial in the quest of a unified view of the insulator-to-metal transition in strongly correlated systems, since it is the only means to span all the possible band fillings. In this spirit, the Mott transition occurring at the “most” commensurate filling $n = 1$ and the Wigner crystal at $n \rightarrow 0$ are intimately connected, and can be viewed as two limiting cases of the same general phenomenon.

Acknowledgments

We wish to thank F. Nad and J.-P. Pouget for fruitful discussions. One of us (B.V.) is very grateful to M.A.H Vozmediano for valuable discussions. Financial support from MEC (Spain) through Grant No. PB96/0875 and CAM (Madrid) through Grant No. 07/0045/98 is acknowledged. This work has also been supported by the Swiss National Foundation through grant no. 20-61470.00.

APPENDIX A: VARIATIONAL ENERGY AT QUARTER-FILLING

In this appendix we will detail the computation of the ground-state energy for the quarter-filled case $n = N/L = 1/2$, using the trial ground state (24). We have to evaluate the three terms

$$E_{BG}(\eta, \lambda) = -t\langle\hat{T}\rangle + U\langle\hat{D}\rangle + V\langle\hat{W}\rangle, \quad (\text{A1})$$

where

$$\langle\hat{O}\rangle = \frac{\langle\Psi_\infty|e^{-\eta\hat{T}}e^{-\lambda\hat{D}}\hat{O}e^{-\lambda\hat{D}}e^{-\eta\hat{T}}|\Psi_\infty\rangle}{\langle\Psi_\infty|e^{-\eta\hat{T}}e^{-2\lambda\hat{D}}e^{-\eta\hat{T}}|\Psi_\infty\rangle}. \quad (\text{A2})$$

Besides the variational parameters η and λ , the wave function $|\Psi_\infty\rangle$ itself is not known *a priori*, but has also to be determined by minimizing the energy. It will turn out that $|\Psi_\infty\rangle$ is the ground state of the 1D Heisenberg antiferromagnet, with spins located on even (or odd) sites. We use an expansion in powers of η and therefore have to

assume that V is large enough to keep the electrons close to their positions in the classical limit. As the analysis is straightforward, we only indicate the main steps.²⁷

1. Kinetic energy

Expanding to fourth order in η we obtain for the mean value of the kinetic energy

$$\begin{aligned} \langle \hat{T} \rangle = & -2\eta \langle \Psi_\infty | \hat{T}^2 | \Psi_\infty \rangle - \frac{4}{3}\eta^3 \langle \Psi_\infty | \hat{T}^4 | \Psi_\infty \rangle + \\ & -\eta^3 \langle \Psi_\infty | \hat{T}^2 (e^{-\lambda \hat{D}} - 1) \hat{T}^2 | \Psi_\infty \rangle + \\ & + 4\eta^3 (\langle \Psi_\infty | \hat{T}^2 | \Psi_\infty \rangle)^2. \end{aligned} \quad (\text{A3})$$

To proceed we have to compute correlation functions of the type $\langle \Psi_\infty | \hat{T}^{2m} | \Psi_\infty \rangle$ (all contributions with odd exponents vanish). The operator \hat{T}^{2m} can be decomposed using Wick's theorem. The expectation value of the squared kinetic energy operator ($m = 1$) is easily computed and gives $\langle \Psi_\infty | \hat{T}^2 | \Psi_\infty \rangle = L$. The expectation value of the fourth power of the kinetic energy is more involved, but it is easy to see that only terms with two or three contractions contribute. These can be expressed in terms of density operators n_i and spin $\frac{1}{2}$ operators \vec{S}_i , giving

$$\frac{1}{3} \langle \Psi_\infty | \hat{T}^4 | \Psi_\infty \rangle = L^2 - \sum_{i \text{ even}} \langle \Psi_\infty | 4\vec{S}_i \cdot \vec{S}_{i+2} - n_i n_{i+2} | \Psi_\infty \rangle. \quad (\text{A4})$$

The term L^2 is cancelled by a corresponding term coming from the denominator of eq. (A2), so that only “linked diagrams” contribute to the expectation value of the kinetic energy. In order to calculate the remaining term in eq. (A3), we notice that only the first and third processes in fig. 7 contribute. We obtain

$$\begin{aligned} (e^{-\lambda \hat{D}} - 1) \hat{T}^2 | \Psi_\infty \rangle = \\ (e^{-\lambda} - 1) \left[\sum_{i \text{ odd}, \sigma} c_{i\sigma}^+ c_{i+\sigma} c_{i\bar{\sigma}}^+ c_{i-\sigma} | \Psi_\infty \rangle + \right. \\ \left. \sum_{i \text{ even}, \sigma} c_{i\sigma}^+ c_{i+\sigma} c_{i+\sigma}^+ c_{i+2\sigma} | \Psi_\infty \rangle \right]. \end{aligned} \quad (\text{A5})$$

Using again the Wick decomposition and the representation of the remaining fermionic operators in terms of spin and density operators, we find

$$\begin{aligned} \langle \Psi_\infty | \hat{T}^2 (e^{-\lambda \hat{D}} - 1) \hat{T}^2 | \Psi_\infty \rangle = \\ -3(e^{-\lambda} - 1) \sum_{i \text{ even}} \langle \Psi_\infty | 4\vec{S}_i \cdot \vec{S}_{i+2} - n_i n_{i+2} | \Psi_\infty \rangle \end{aligned} \quad (\text{A6})$$

Collecting all the terms in Eq. (A3) we arrive at

$$\langle \hat{T} \rangle = -2\eta L + \eta^3 (1 + 3e^{-\lambda}) \sum_{i \text{ even}} \langle \Psi_\infty | 4\vec{S}_i \cdot \vec{S}_{i+2} - n_i n_{i+2} | \Psi_\infty \rangle. \quad (\text{A7})$$

2. On-site interaction energy

The expansion in η of the mean value of the on-site interaction energy gives

$$\langle \hat{D} \rangle = \frac{1}{4} \langle \Psi_\infty | \hat{T}^2 \hat{D} e^{-2\lambda \hat{D}} \hat{T}^2 | \Psi_\infty \rangle \eta^4 + O(\eta^6) \quad (\text{A8})$$

and can be immediately evaluated by comparison with eq. (A6),

$$\langle \hat{D} \rangle = -\frac{3}{4} \eta^4 e^{-2\lambda} \sum_{i \text{ even}} \langle \Psi_\infty | 4\vec{S}_i \cdot \vec{S}_{i+2} - n_i n_{i+2} | \Psi_\infty \rangle. \quad (\text{A9})$$

3. Long-range potential energy

To compute the expectation value $\langle \hat{W} \rangle$ of the long-range potential, we first recall that $|\Psi_\infty\rangle$ is an eigenstate of \hat{W} , namely (for an overall neutral system)

$$\hat{W} |\Psi_\infty\rangle = -\frac{L}{4} \log 2 |\Psi_\infty\rangle. \quad (\text{A10})$$

For $\hat{W}' = \hat{W} + (L/4) \log 2$ all the terms where \hat{W}' acts directly on the wave function are thus suppressed and we have to evaluate only four terms to order η^4 ,

$$\begin{aligned} \langle \Psi_\infty | e^{-\eta \hat{T}} e^{-\lambda \hat{D}} \hat{W}' e^{-\lambda \hat{D}} e^{-\eta \hat{T}} | \Psi_\infty \rangle = \eta^2 \langle \Psi_\infty | \hat{T} \hat{W}' \hat{T} | \Psi_\infty \rangle + \\ + \eta^4 \left\{ \frac{1}{6} (\langle \Psi_\infty | \hat{T} \hat{W}' \hat{T}^3 | \Psi_\infty \rangle + \langle \Psi_\infty | \hat{T}^3 \hat{W}' \hat{T} | \Psi_\infty \rangle) + \right. \\ \left. + \frac{1}{4} \langle \Psi_\infty | \hat{T}^2 e^{-\lambda \hat{D}} \hat{W}' e^{-\lambda \hat{D}} \hat{T}^2 | \Psi_\infty \rangle \right\} + O(\eta^6). \end{aligned} \quad (\text{A11})$$

In this case all the three processes in fig. 7 contribute. An additional complication is the long-range nature of the potential which requires the summation of infinite series. The first three terms of the r.h.s. of eq. (A11) can be linked to previously calculated expressions in view of the relation

$$\hat{W}' \hat{T} | \Psi_\infty \rangle = (2 \log 2 - 1) \hat{T} | \Psi_\infty \rangle. \quad (\text{A12})$$

The last term in eq. (A11) is found to be

$$\begin{aligned} \langle \Psi_\infty | \hat{T}^2 e^{-\lambda \hat{D}} \hat{W}' e^{-\lambda \hat{D}} \hat{T}^2 | \Psi_\infty \rangle = \\ 4[(2 \log 2 - 1)L^2 + (\frac{11}{2} - 10 \log 2)L] + \\ (\frac{15}{2} - 8 \log 2) e^{-2\lambda} \sum_{i \text{ even}} \langle \Psi_\infty | 4\vec{S}_i \cdot \vec{S}_{i+2} - n_i n_{i+2} | \Psi_\infty \rangle. \end{aligned} \quad (\text{A13})$$

Terms proportional to L^2 are again cancelled by terms from the denominator. Adding the contribution (A10) we finally get

$$\begin{aligned} \langle \hat{W} \rangle = & -\frac{L}{4} \log 2 + L(2 \log 2 - 1) \eta^2 \\ & + \left[1 - 2 \log 2 + \left(\frac{15}{8} - 2 \log 2 \right) e^{-2\lambda} \right] \eta^4 \\ & \times \sum_{i \text{ even}} \langle \Psi_\infty | 4\vec{S}_i \cdot \vec{S}_{i+2} - n_i n_{i+2} | \Psi_\infty \rangle. \end{aligned} \quad (\text{A14})$$

-
- ¹ E. Wigner, Trans. Farad. Soc. Lond. **34**, 678 (1938).
- ² J. Hubbard, Phys. Rev. B **17**, 494 (1978).
- ³ S. Aubry, J. Phys. (France) **16**, 2497 (1983).
- ⁴ D. Baeriswyl, in *Nonlinearity in Condensed Matter*, eds. A.R. Bishop *et al.*, Springer Series in Solid State Sciences **69**, 183 (1987).
- ⁵ M. Dzierzawa, D. Baeriswyl and L.M. Martelo, Helv. Phys. Acta **70**, 124 (1997).
- ⁶ Y. Noda and M. Imada, Phys. Rev. Lett. **89**, 176803 (2002).
- ⁷ S. Capponi, D. Poilblanc and T. Giamarchi, Phys. Rev. B **61**, 13410 (2000); D. Poilblanc, S. Yunoki, S. Maekawa and E. Dagotto, Phys. Rev. B **56**, R1645 (1997).
- ⁸ H.J. Schulz, G. Cuniberti and P. Pieri, in *Field Theories for Low-Dimensional Condensed Matter Systems*, eds. G. Morandi *et al.*, Springer-Verlag, Berlin (2000).
- ⁹ H.J. Schulz, Phys. Rev. Lett. **71**, 1864 (1993).
- ¹⁰ D.M. Ceperley and B.J. Alder, Phys. Rev. Lett. **45**, 566 (1980); B. Tanatar and D.M. Ceperley, Phys. Rev. B **39**, 5005 (1989).
- ¹¹ C. Aebischer, D. Baeriswyl and R.M. Noack, Phys. Rev. Lett. **86**, 468 (2001).
- ¹² See, e.g., F. Nad, P. Monceau, C. Carcel and J.M. Fabre, Phys. Rev. B **62**, 1753 (2000).
- ¹³ K. Hiraki and K. Kanoda, Phys. Rev. Lett. **80**, 4737 (1998).
- ¹⁴ S. Brazovskii, N. Kirova and P. Monceau, eds., *International Workshop on Electronic Crystals (ECRYS-2002)*, J. Phys. (France) IV **12**, Pr9 (2002).
- ¹⁵ H. Otsuka, J. Phys. Soc. Jpn. **61**, 1645 (1992).
- ¹⁶ M. Dzierzawa, D. Baeriswyl and M. Di Stasio, Phys. Rev. B **51**, 1993 (1995).
- ¹⁷ L. Hulthén, Arkiv Mat. Astron. Fysik **26A**, 1 (1938).
- ¹⁸ A. Auerbach, *Interacting Electrons and Quantum Magnetism*, Springer-Verlag, New York 1994.
- ¹⁹ D.S. Chow, F. Zamborszky, B. Alavi, D.J. Tantillo, A. Baur, C.A. Merlic and S.E. Brown, Phys. Rev. Lett. **85**, 1698 (2000).
- ²⁰ P. Monceau, F.Ya. Nad and S. Brazovskii, Phys. Rev. Lett. **86**, 4080 (2001).
- ²¹ K.C. Ung, S. Mazumdar and D. Toussaint, Phys. Rev. Lett. **73**, 2603 (1994).
- ²² F. Mila, Phys. Rev. B **52**, 4788 (1995).
- ²³ H. Seo and H. Fukuyama, J. Phys. Soc. Jpn. **66**, 1249 (1997).
- ²⁴ C.S. Jacobsen, J. Phys. C **19**, 5643 (1986).
- ²⁵ J.P. Pouget, Phys. Rev. Lett. **37**, 437 (1976).
- ²⁶ F. Castet, A. Fritsch and L. Ducasse, J. Phys. (France) I **6**, 583 (1996).
- ²⁷ For more details see B. Valenzuela, Ph.D. thesis, Madrid (2002), unpublished.
- ²⁸ For more complex fillings such as $n = r/s$, the expression for the gap is not as simple as eq. (6). The occupied sites are not all equivalent, and leakage to a wrong site now depends crucially on the local environment. Expression (7) can still be considered as a rough estimate for the general case, although sensible variations can be expected when moving from simple commensurabilities such as $n = 1/2$ or $n = 1/3$ to more complex charge patterns.
- ²⁹ For weak interactions, a better estimate for the ground-state energy can in principle be obtained using
- $$|\Psi_G(\lambda)\rangle = e^{-\lambda\hat{W}}|\Psi_0\rangle,$$
- where $|\Psi_0\rangle$ is the Fermi sea. The operator $e^{-\lambda\hat{W}}$ builds up the charge correlations appropriate for the GWL, by enhancing the configurations with low interaction energy. This wave function can be considered as the “dual” of $|\Psi_B\rangle$ and is always metallic. Direct comparison of the two complementary approaches is expected to give a good description of charge ordering. However, the calculation of the variational energy $E_G(\lambda)$ is not simple when dealing with long-range interactions, and will be left for future work.
- ³⁰ The distance m between sites i and j is defined as $m = |i - j|$, the linear distance. Other choices are possible. For instance, taking m to be the chord distance on the circle [G. Fano, F. Ortolani, A. Parola and L. Ziosi, Phys. Rev. B **60**, 15654 (1999); Y. Hatsugai, Phys. Rev. B **56**, 12183 (1997)] slightly modifies the function $V(q)$ — which can no longer be expressed in closed analytical form — but has the advantage of avoiding multiple counting by construction.
- ³¹ The charge gap in the strong-coupling limit can be evaluated in general for models with m -neighbor interactions. The largest value is obtained for $m = 1$ (only n.n. interactions), $\Delta_1 = V$, and the lowest is for $m = 2$ (n.n.n. interactions), $\Delta_2 = 0$. The gap for larger m converges to the value $\Delta_\infty = 0.39$ given by eq. (6) with an oscillatory behavior.
- ³² A similar expansion has been successfully used for the Hubbard chain at half filling, where one correctly obtains the Heisenberg antiferromagnet with exchange constant $J = 4t^2/U$.⁴
- ³³ Note that, in contrast to spin correlations, which vanish for $U \rightarrow \infty$, density correlations depend only weakly on U for small t (and therefore small η). In fact, it is easy to show that up to second order in η the static structure factor is identical to that of spinless fermions (i.e., to the limit $U \rightarrow \infty$).